Visible light photocatalytic H_2-production activity of wide band gap ZnS nanoparticles based on the photosensitization of graphene

2015 Nanotechnology 26 345402

(http://iopscience.iop.org/0957-4484/26/34/345402)

IOP Publishing Nanotechnology

Nanotechnology **26** (2015) 345402 (8pp) doi:10.1088/0957-4484/26/34/345402

Visible light photocatalytic H_2-production activity of wide band gap ZnS nanoparticles based on the photosensitization of graphene

Faze Wang[1], **Maojun Zheng**[1,2], **Changqing Zhu**[1], **Bin Zhang**[1], **Wen Chen**[1], **Li Ma**[3] **and Wenzhong Shen**[1]

[1] Key Laboratory of Artificial Structure and Quantum Control, Ministry of Education, Department of Physics and Astronomy, Shanghai Jiao Tong University, Shanghai, 200240, People's Republic of China
[2] Collaborative Innovation Center of Advanced Microstructures, Nanjing University, Nanjing, 210093, People's Republic of China
[3] School of Chemistry and Chemical Technology, Shanghai Jiao Tong University, Shanghai, 200240, People's Republic of China

E-mail: mjzheng@sjtu.edu.cn

Received 1 April 2015, revised 19 June 2015
Accepted for publication 13 July 2015
Published 5 August 2015

Abstract

Visible light photocatalytic H_2 production from water splitting is considered an attractive way to solve the increasing global energy crisis in modern life. In this study, a series of zinc sulfide nanoparticles and graphene (GR) sheet composites were synthesized by a two-step hydrothermal method, which used zinc chloride, sodium sulfide, and graphite oxide (GO) as the starting materials. The as-prepared ZnS-GR showed highly efficient visible light photocatalytic activity in hydrogen generation. The morphology and structure of the composites obtained by transmission electron microscope and x-ray diffraction exhibited a small crystallite size and a good interfacial contact between the ZnS nanoparticles and the two-dimensional (2D) GR sheet, which were beneficial for the photocatalysis. When the content of the GR in the catalyst was 0.1%, the ZG0.1 sample exhibited the highest H_2-production rate of 7.42 μmol h^{-1} g^{-1}, eight times more than the pure ZnS sample. This high visible-light photocatalytic H_2 production activity is attributed to the photosensitization of GR. Irradiated by visible light, the electrons photogenerated from GR transfer to the conduction band of ZnS to participate in the photocatalytic process. This study presents the visible-light photocatalytic activity of wide bandgap ZnS and its application in H_2 evolution.

Keywords: zinc sulfide, nanoparticles, graphene, visible light photocatalyticactivity, hydrogen generation

(Some figures may appear in colour only in the online journal)

1. Introduction

Nowadays, the environmental pollution caused by burning fossil fuels and the global energy crisis have become more and more serious. Photoelectrochemical (PEC) splitting of water using solar energy for H_2 has attracted considerable attention, as H_2 is a renewable and green energy carrier. Since the pioneering report by Fujishima and Honda on PEC water splitting on a TiO_2 electrode [1], various active photocatalysts such as oxide, sulfide, and oxynitride semiconductors have been developed as photocatalysts for the water-splitting reaction [2]. ZnS is a well-known photocatalyst among all these material. It shows high activity for H_2 evolution, because it generates electron hole pairs under light irradiation rapidly and has a high negative potential for exciting electrons, even without the assistance of any noble metal cocatalysts [3]. However, ZnS can solely absorb ultraviolet (UV) light, which accounts for only 4% of total sunlight due to its large bandgap of 3.66 eV. Numerous attempts such as doping metal ions (Au [4], Cu [5, 6], Ni [7], Pb [8], and Sr [9]) and preparation of solid solutions have been applied to make ZnS generate visible-light activity [10–16]. Unfortunately, heavy-metal cadmium and lead are toxic and harmful to human beings and the environment, which limits their wide application. Hence, it is highly desirable to develop low-toxic and cost-effective ZnS-based photocatalysts with high H_2 production activities under visible light.

Graphene, a two-dimensional (2D) network of carbon materials, has been reported to as an efficient photocatalytic H_2 production cocatalyst [17–25]. Owing to the abundance of delocalized electrons from the conjugated sp^2-bonded carbon network, graphene enhances the transportation of electrons photogenerating in semiconductor particles. Some GR-based semiconductors have been fabricated to enhance photocatalytic performance. Nevertheless, GR has been widely considered as an electron reservoir and transfer and acts as an electron transfer channel to reduce the recombination of photogenerated electron holes, leading to improved photoconversion efficiency of photocatalytic materials [26]. Meanwhile, it has always been proposed that GR cannot narrow the bandgap of a semiconductor to produce visible-light photocatalytic activity. Zhang *et al* reported a visible-light-response ZnS/reduced graphene oxide (RGO) photocatalyst recently and proved that RGO in the nanocomposites acts as an organic dye-like macromolecular 'photosensitizer' [27]. The photogenerated electrons from GR upon visible-light irradiation can transfer to the conduction band of ZnS, while ZnS itself is not bandgap-photoexcited. Through the photosensitization process of GR, the wide-bandgap ZnS exhibits visible-light photoactivity toward the selective aerobic oxidation process. Herein, we prepared the ZnS-GR nanocomposites, further expanded its application in hydrogen generation, and investigated its visible-light, photoactive H_2 production activity. The influences of GR content on the photocatalytic activity of ZnS-GR composites were discussed. Compared to that of pure ZnS, the optimal ZnS-GR sample containing 0.1% GR exhibits a high rate of H_2 production under visible-light irradiation. The measurements of photocatalytic H_2 production activity directly provide evidence that GR can be a photosensitizer for semiconductors.

2. Experimental setup

2.1. Preparation of graphite oxide (GO) and ZnS-graphene composites

Graphite oxide was synthesized from natural graphite by a modified Hummer's method [28]. Graphite powder (2 g) was mixed with concentrated H_2SO_4 (12 mL), $K_2S_2O_8$ (2.5 g), and P_2O_5 (2.5 g). The reaction was heated to 80 °C in an oil bath. After 24 h stirring, the mixture was filtered and dried under ambient condition overnight. The pre-oxidized graphite was then added to a mixture of concentrated H_2SO_4 (120 mL) and HNO_3 (30 mL), cooling in an ice-water bath. After strong magnetic stirring for 30 min, 15 g $KMnO_4$ was added gradually and reacted for 2 h. Shortly afterwards, the mixture was further diluted with 1 L of deionized (DI) water, 20 mL of 30% H_2O_2 was added to the mixture, and a brilliant yellow product was formed along with bubbling, followed by washing with a HCl (1:10) aqueous solution and DI water. The solid obtained on the filter was dispersed in water under sonication by an ultrasonic processor, giving a bright yellow GO solution.

In a typical synthesis of the composite, 0.205 g $ZnCl_2$ and GO were dispersed into distilled water (50 ml), and this solution was heated to 60 °C in an oil bath with continuous stirring for 2 h. Subsequently, 0.10 M Na_2S (20 ml) solution was added dropwise and kept stirring for 4 h. After that, the suspension was transferred to a 100 mL Teflon-lined autoclave and maintained at 130 °C for 12 h. The final products with different weight addition ratios of GO were rinsed three times by distilled water and ethanol and dried at 60 °C in a vacuum oven for 10 h.

2.2. Materials characterizations

Atomic force microscopic (AFM, Nanoscope III MultiMode SPM) measurements were performed to characterize the GO sheet thickness and dimensions. The crystalline structure of the ZnS-GR powder products was determined by x-ray diffraction (XRD, D8 DISCOVER x-ray diffractometer, Bruker, Karlsruhe, Germany) with Cu Kα radiation (1.54 Å). The surface composition of the sample was analyzed by x-ray photoelectron spectroscopy (XPS, AXIS ULTRA DLD, Kratos, Japan). Raman spectroscopy was recorded on Renishaw in a Via-reflex system at room temperature. A laser wavelength of 532 nm was used as the excitation source.

The photoluminescent (PL) spectra were measured by the Jobin Yvon LabRam HR 800 UV system (Horiba, Kyoto, Japan) at room temperature. A laser wavelength of 514.5 nm was used as the excitation source. The morphology and microscopic structure information were determined by transmission electron microscopy (TEM, JEM-2100F, JEOL Ltd, Japan). Absorption spectra of the samples were obtained by using a UV/vis spectrometer (Lambda 950, Perkin Elmer, Inc., USA) over a wavelength range of 250–600 nm. $BaSO_4$ was employed as the internal reflectance standard.

2.3. Photocatalytic hydrogen evolution and electrochemical measurements

The photocatalytic performance of the synthesized photocatalysts was investigated in a gas-closed circulation system (Labsolar-III, Beijing Perfectlight Technology Co., Ltd, Beijing, China) with a top-window Pyrex cell. A 300 W Xe lamp (SOLAREDGE700, Beijing Perfectlight Technology Co., Ltd, Beijing, China) equipped with a UV cut off filter ($\lambda > 420$ nm) was used as the light source. The amount of H_2 evolved was analyzed by an online gas chromatograph (GC7900, Techcomp Ltd, China; TCD, N_2 as a carrier gas and MS-5A column). In a typical photocatalytic experiment, 50 mg of catalysts were dispersed in 50 mL of mixed aqueous solution containing 0.35 M Na_2S and 0.25 M Na_2SO_3 with constant stirring. Before irradiation, the system was bubbled under vacuum condition to remove the dissolved air.

Photoelectrochemical measurements were performed using a PARSTAT 4000 workstation with a standard three-electrode system, using the prepared samples as the working electrodes, Pt gauze as the counter electrode, and Ag/AgCl as a reference electrode. The working electrode was prepared on an F-doped SnO_2-coated (FTO) conductor glass. 0.2 g of ZnS-GR composite was ground with 0.06 g polyethylene glycol (molecular weight: 20 000) and 0.5 mL of water to make a slurry. The slurry was spread onto an FTO glass by the doctor-blade method. The working electrode was dried in a vacuum oven at 60 °C. The electrolyte was a mixture solution of 0.35 M Na_2S and 0.25 M Na_2SO_3 ($pH = 13.5$). A 300 W Xe lamp system equipped with a UV cutoff filter ($\lambda > 420$ nm) (SOLARDGE 700, Beijing Perfectlight Technology Co., Ltd, China) was used as the light source.

3. Results and discussion

The ZnS-GR composites were fabricated via a two-step process in a solution phase. First, $ZnCl_2$ was added into a single-layer GO dispersed solution. During this step, the Zn^{2+} can be adsorbed onto the negatively charged GO surface by electrostatic attraction [29]. Subsequently, GO was reduced to GR by a hydrothermal reduction treatment, and ZnS nanoparticles were simultaneously formed on the GR sheets. The weight ratios of GO to ZnS were 0, 0.05, 0.1, 0.25, 0.5, 1, and 3%, and the corresponding samples were labeled as ZG0, ZG0.05, ZG0.1, ZG0.25, ZG0.5, ZG1, and ZG3, respectively. GR was prepared by the reduction of graphene oxide. Notably, after strong ultrasonication for 15 min, monolayer graphene sheets were peeled off from the GO and stably dispersed in the bright yellow solution. The AFM images (figure 1) show the thickness of the graphite oxide is about 0.8 nm, which is comparable to the literature data (0.737 nm) of the single-layer GO nanosheet as reported before, indicating that most of the GO are flat and monolayer [30]. Figure 2(c) shows the XRD patterns of as-prepared ZnS-GR composites. The peaks at 28.5, 47.5, and 52.1 correspond to the diffractions of the (111), (220), and (311) planes of cubic ZnS (JCPDS 05-0566) [31]. For the photocatalysts with different weight addition ratios of GR, they show similar XRD patterns with blank ZnS, implying that GR does not have a significant influence on the phase structure and crystallinity of ZnS-GR samples. No characteristic diffraction peaks for GO and GR can be observed on these patterns because of the low amount and relatively low diffraction intensity.

The morphologies and microstructures of the samples were examined by TEM. It can be seen from figure 2(a) that nanosized ZnS particles spread uniformly on the surface of the GR sheet support. The size of the ZnS nanocrystals is around 5 nm. The high-resolution TEM (HR-TEM) image (figure 2(b)) shows that the detail of the lattice of the nanocrystals with an interplanar spacing is 0.31 nm, corresponding to the (111) plane of cubic ZnS. Three distinct diffraction rings are seen from the selected-area electron diffraction (SAED) pattern in figure 2(b) and can be indexed to the (111), (220), and (311) crystal lattice of ZnS, which is consistent with the XRD results. The TEM characterization suggests that a good interfacial contact is formed between the ZnS nanoparticles and the 2D GR sheet, which is helpful for improving the charge separation and thus the photocatalytic activity.

After hydrothermal treatment, the efficient reduction of GO to GR was also evidenced by high-resolution C1s x-ray photoelectron spectra (XPS) of GO and ZG0.1. A signal deconvolution with Gaussian-curve fitting points out chemically different C species. For the GO, two typical peaks are located at 284.6 and 286.7 eV (figure 3(a)), which are usually assigned to adventitious carbon and sp^2-hybridized carbon from the GO and the oxygen-containing carbonaceous bonds (C–OH). The strong peak for C–OH bonds indicates an efficient oxygenation of graphite by a modified Hummer's method. Such a surface functional group can provide more active sites for connection with ZnS nanoparticles. For the ZG0.1 nanocomposite, the spectrum is deconvoluted into four peaks, and the significant loss of oxygen-containing functional groups is observed in figure 3(b). The sharp peak for C–O almost vanishes, and the peaks for C=O and O=C–O still exist but have much lower intensities than those in GO, which indicate the sufficient reduction of GO to GR after the hydrothermal reduction treatment of Na_2S. The hydrothermal reaction process from GO to GR is also investigated in Raman spectra. Figure 2(d) shows a comparison of the Raman spectra of GO and the ZnS-GR composite (sample ZG0.1). The D band at around 1355 cm^{-1} is common for disordered sp^2 carbon, while the G band at around 1600 cm^{-1} is usually assigned to well-ordered graphite. After hydrothermal treatment at 130 °C for 12 h, the ratio of the intensities of the D and G bands (ID/IG) increases from 0.81 to 0.91. The change in the ID/IG ratio suggests a decrease in the average size of the re-established G network (sp^2 carbon), further confirming the reduction of GO [32–35].

Figure 4 shows the UV–vis absorption spectra of the samples ZGx ($x = 0$, 0.1, 0.25, 0.5, 1, and 3). For all the samples studied, a wide background absorption in the visible-light region ranging from 400–800 nm is observed, and such absorption gradually increases with the increasing of GO content. It is in accordance with the powder color changing from white to gray. The bandgap of ZnS-GR composites can be acquired from plots of $(\alpha E_{\text{photon}})^2$ versus the energy (E_{photon}) of absorbed light (α and E_{photon} are the absorption coefficient and the discrete photon energy, respectively). The extrapolated value (a straight line to the x-axis) of E_{photon} at $\alpha = 0$ gives absorption edge energies corresponding to e.g. from figure 4(b), the bandgap of the synthesized ZGx is 3.40 eV, 3.36 eV, 3.31 eV, and 3.27 eV, corresponding to ZG0, ZG0.25, ZG1, and ZG3, respectively. This result shows a bandgap narrowing of the semiconductor because of the coupling in ZnS-GR nanocomposites. According to the reported literature [36–40], this result can be attributed to the hybridization of carbon materials. Due to the substitutional nature of the incorporated carbon, carbon doping into the ZnS lattice creates midgap energy levels with inducing a decrease in bandgap energy.

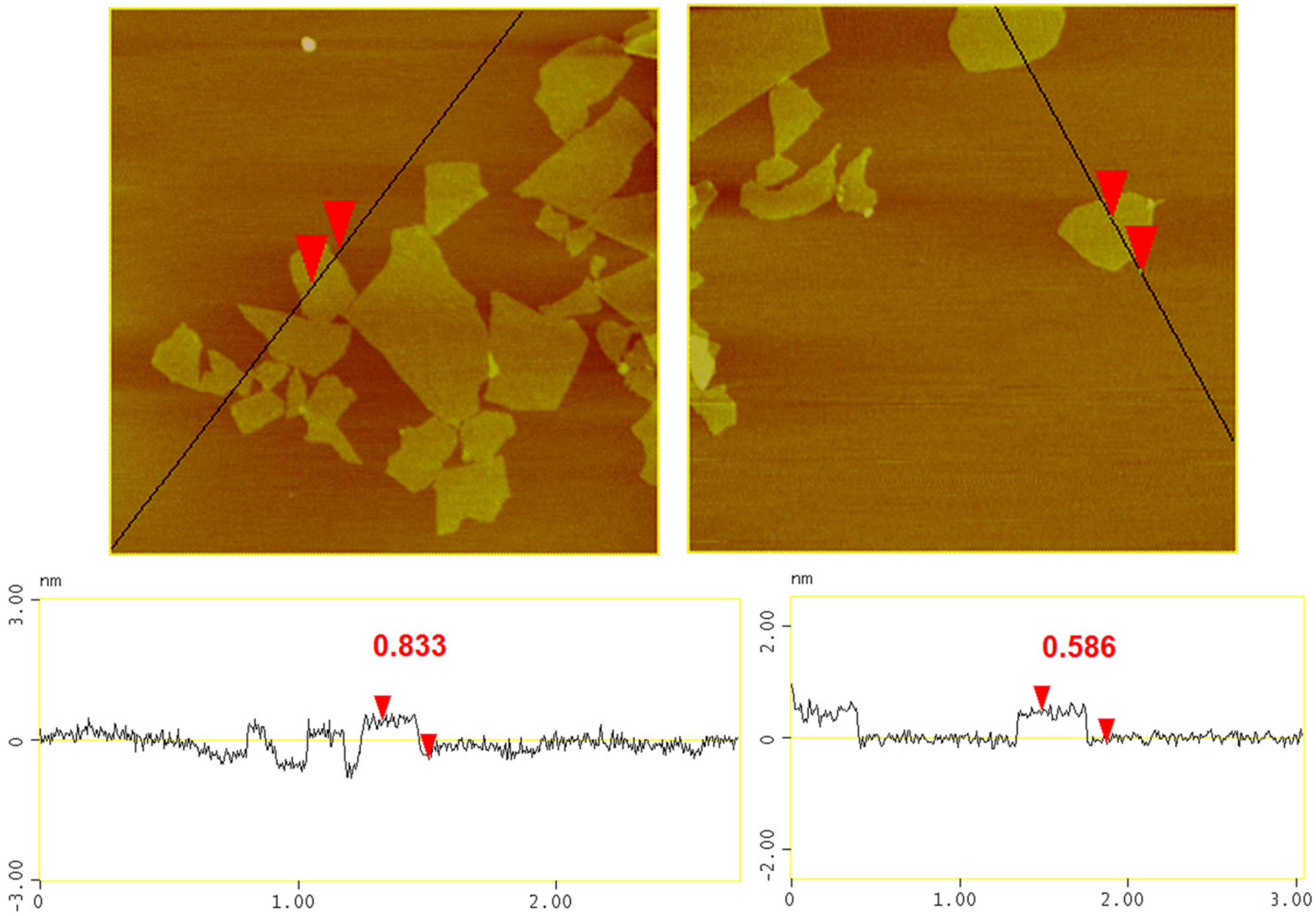

Figure 1. AFM images and height profiles of a single layer of GO.

The photocatalytic H_2 production activity of the ZnS-GR nanocomposites from an aqueous solution containing 0.35 M Na_2S and 0.25 M Na_2SO_3 under visible-light irradiation ($\lambda > 420$ nm) is given in figure 5. The sacrificial reagent may decrease the rate of hole–electron recombination and increase the active number of injected electrons. As can be seen from this figure, the graphene content has a significant influence on the photocatalytic activity of ZnS. After introducing only a small amount of graphene, the activity of the ZGx sample is remarkably enhanced. The rate of H_2 evolution increases with the increasing of GR content, achieving a maximum of 7.42 μmol h^{-1} g^{-1} at the GR content of 0.1 wt%. This value is about eight times higher than pure ZnS. When graphene content is higher than 0.1 wt%, a further increase in graphene content leads to a reduction of the photocatalytic activity. Especially, at a graphene content of 1 wt%, the photocatalytic activity of the sample ZG1 has a drastic decrease. The reasons may be that excessive GR lowers the intensity of incident light and increases the opportunity for recombination of the photo-generated electron–hole pairs. After 10 h light irradiation, the sample of ZG0.1 does not exhibit any loss of activity, indicating the better stability of this nanocomposite for hydrogen generation. The high stability of the ZG0.1 catalyst is attributed to the finite-size effect that the high-symmetry crystalline phase is more stable at a smaller size.

As mentioned above, the UV–vis absorption spectra ZnS-GR indicates that the wide bandgap of ZnS is narrowed to some degree. However, this bandgap is still so large that ZnS-GR should not exhibit visible-light photoactivity. Normally, the VB electrons (e^-) of ZnS cannot be excited to CB, and the samples ZGx should have a very low photocatalytic activity under visible irradiation. On the contrary, the ZnS-GR composite photocatalyst shows high photocatalytic H_2 production activity for the sample containing 0.1% GR. Thus, a tentative mechanism of the photocatalytic reaction is proposed that GR acts as an organic dye-like macromolecular ‘photosensitizer’. As illustrated in the figure 6, the electrons on the highest occupied molecular orbital (HOMO) of graphene were at first excited to the lowest unoccupied molecular orbital (LUMO) of graphene under visible-light irradiation, then the photoinduced electrons in graphene were injected to the CB of ZnS, leading to the hole–electron separation. The electrons transferred to the surface of the semiconductor and reacted with the adsorbed H^+ ions to form H_2, producing the visible-light activity [41–44]. Such a H_2 production activity measurement is direct evidence of the existence of injected electrons under visible irradiation and proves GR acting as a photosensitizer. In addition, the PL spectroscopy (figure 7) measurement of ZnS and ZnS-GR was performed under visible-light irradiation. No PL emission is

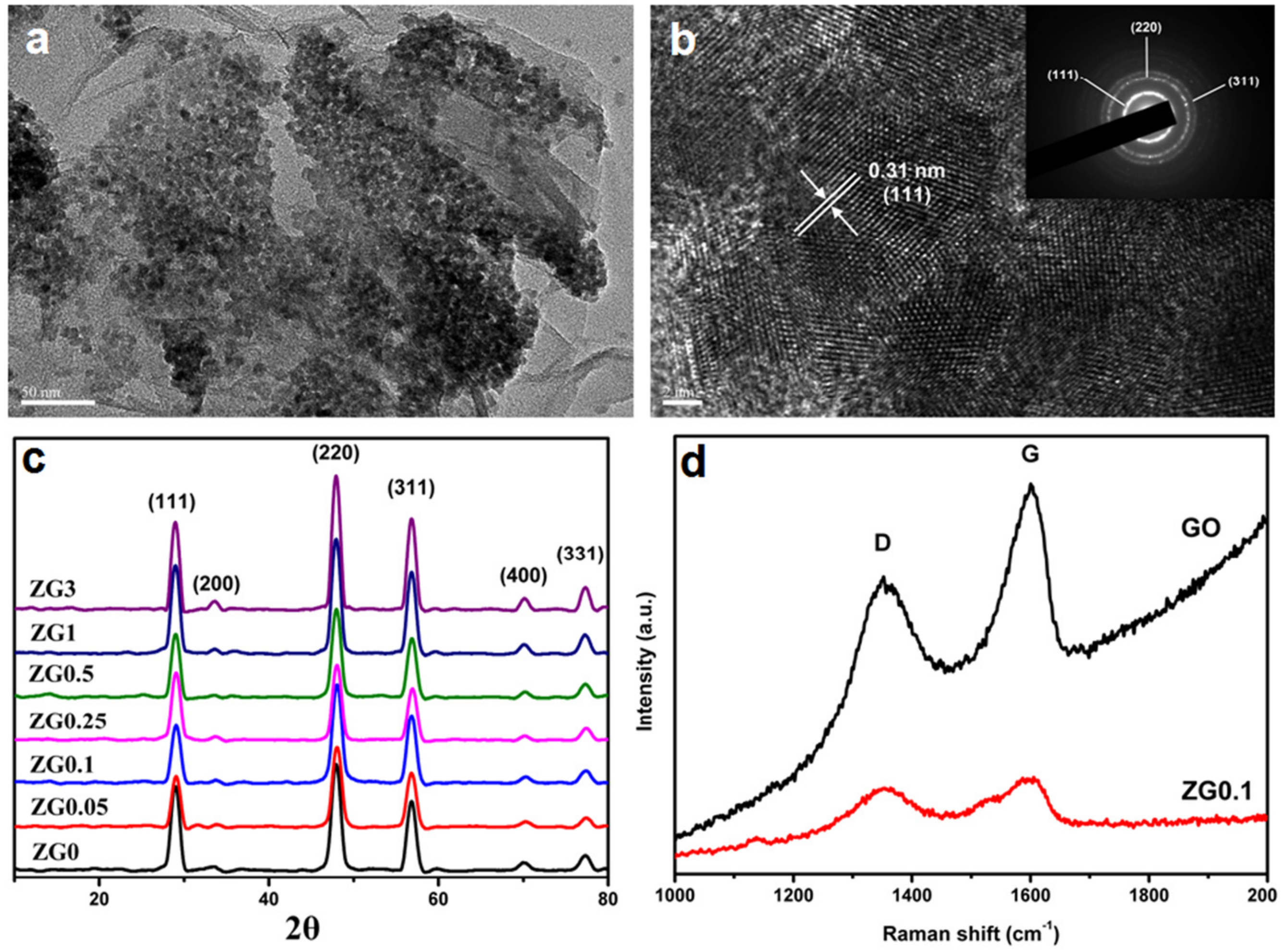

Figure 2. TEM (a) and HR-TEM (b) images of ZG0.1 sample. Inset are the selected area electron diffraction (SAED) patterns corresponding to the ZnS nanoparticles. (c) XRD patterns of the as-prepared ZG*x* photocatalysts with different *x* values. (d) Raman spectra of the GO and ZG0.1 samples.

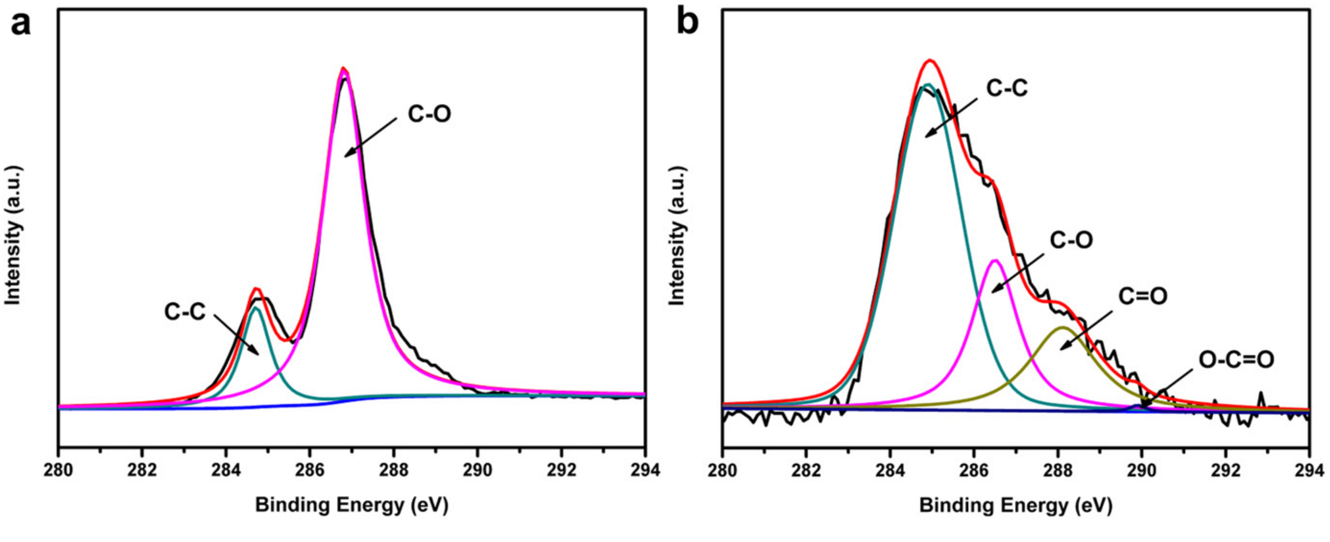

Figure 3. The peak deconvolution of the C (1 s) XPS core level of (a) GO and (b) GR.

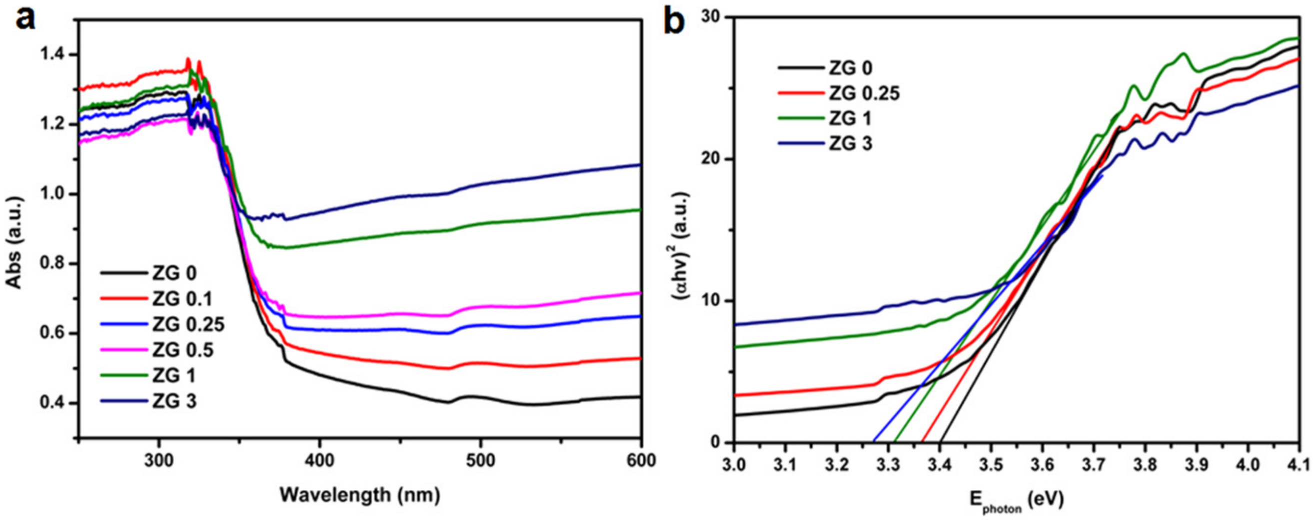

Figure 4. UV–vis absorption spectra (a) and bandgap evaluation (b) from the plots of $(\alpha E_{\mathrm{photon}})^2$ versus E_{photon}.

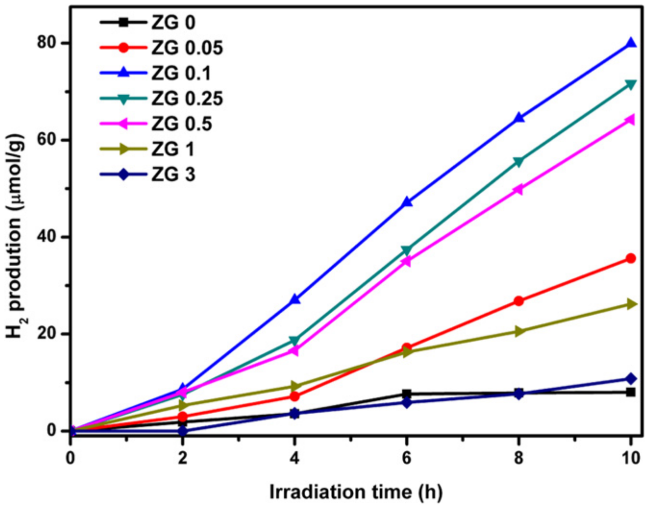

Figure 5. Photocatalytic H_2 evolution of the obtained ZG*x* composites with different GR content under visible light ($\lambda > 420$ nm).

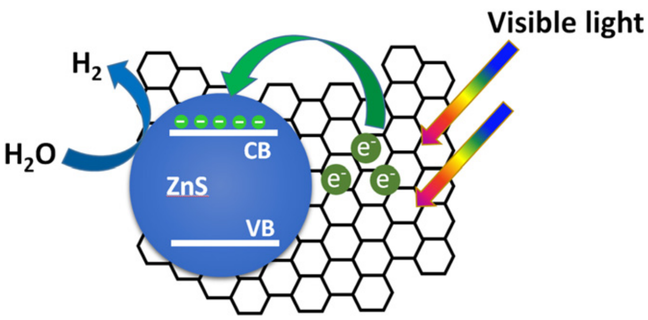

Figure 6. Schematic illustration of the charge separation and transfer in the ZnS-GR composites under visible-light irradiation.

observed for blank ZnS. Thus, ZnS is not able to reach excited states under visible-light irradiation. However, for ZnS-GR, a peak ranging from 500–700 nm is observed. These results suggest that under visible- light irradiation, the GR in

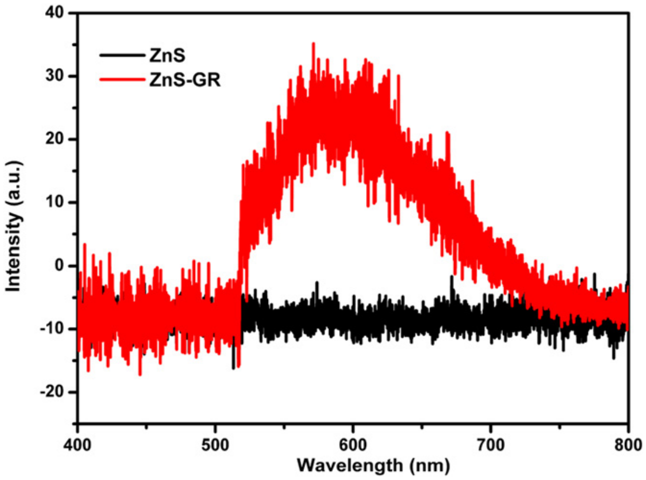

Figure 7. Photoluminescent (PL) spectra of ZnS and ZnS-GR excited at 514.5 nm.

the ZnS-GR nanocomposite can be excited from ground state GR to excited state GR*, and the photoinduced electrons can be transferred to the CB of ZnS, leading to a charge injection and separation. Thus, ZnS-GR is able to show visible-light photoactivity toward hydrogen generation. The ZnS-GR composites with a diameter of 5 nm (figure 8) also offer a larger surface area, which can provide more surface active sites for the adsorption of H^+ ions, making the photocatalytic process more efficient.

To provide additional evidence for the above-suggested photocatalytic mechanism, PEC studies were carried out in a 0.35 M Na_2S and 0.25 M Na_2SO_3 solution (pH = 13.35), acting as both the supporting electrolyte medium and sacrificial reagents. Figure 9 shows the chronoamperometry measurement of ZG0.1 and pure ZnS. The transient photocurrent and responses of ZnS and ZG0.1 are recorded for several on–off cycles of visible irradiation at a bias potential of 0.5 V versus Ag/AgCl. As seen from figure 9, for blank ZnS under visible- light irradiation, almost no photocurrent is

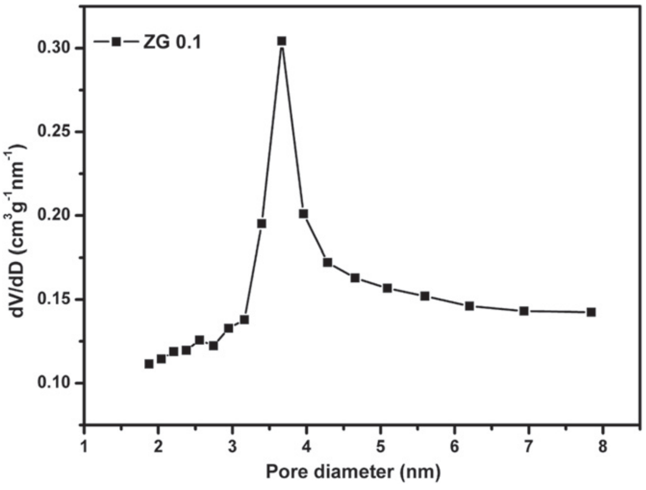

Figure 8. Pore-size distribution curve of ZG0.1 sample.

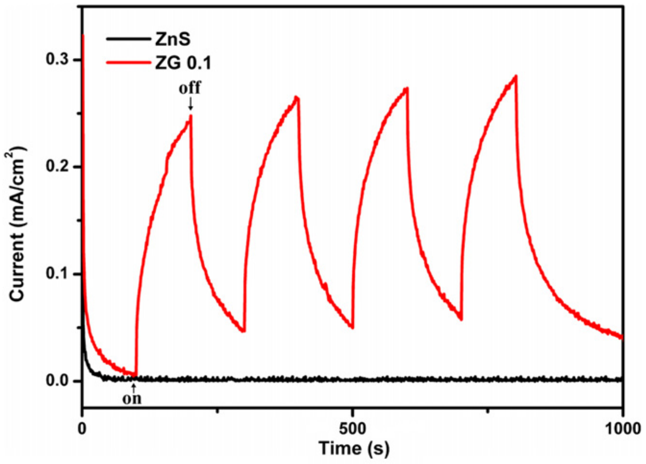

Figure 9. The transient photocurrent responses of the ZG0 and ZG0.1 samples under visible-light irradiation ($\lambda > 420$ nm) at 0.5 V versus Ag/AgCl.

observed within the switch-on and switch-off cycles, because the bare ZnS cannot be photoexcited due to its wide bandgap. For ZG0.1 an apparently boosted photocurrent response appears, and the on–off cycles of the photocurrent are reproducible. The enhancement of the photocurrent indicates that the wide-bandgap ZnS exhibits excellent photocatalytic activity in hydrogen generation under visible-light irradiation owing to the introduction of GR. Moreover, the anodic photocurrent spikes at the beginning of irradiation and the cathodic spikes at the end of irradiation are not visible. The transient photocurrent shows a relatively slow response when the light is switched on and off. The delay is mainly due to the traps of electrons on the surface of ZnS and graphene. Therefore, upon continuous irradiation the further photogenerated electrons from a small amount of graphene gradually fill the traps of ZnS, and only a part of the electrons are transferred to the back of the electrode, which causes a slow current response. Similarly, when the light is switched off, due to the low Fermi level, graphene can store the photogenerated electrons and delay the release of charge carriers from ZnS.

4. Conclusion

In conclusion, the visible-light photocatalytic activity of ZnS-GR composites for H_2 evolution is demonstrated in this paper. A series of ZGx composites with different GR content were synthesized by a two-step hydrothermal method. For the blank ZnS, almost no photocatalytic activity is observed under visible light irradiation, because the wide-bandgap ZnS cannot be photoexcited by visible-light irradiation. However, the as-prepared sample ZnS-GR with 0.1% GR reaches a high photocatalytic H_2 production rate of 7.42 μmol h^{-1} g^{-1} under the same conditions. The results indicate that the unique features of GR make it behave like a photosensitizer rather than an electron reservoir to capture or transfer photogenerated electrons. This study not only demonstrates the visible-light photocatalytic activity of ZnS-GR composites but also further expands the application of a graphene-semiconductor in visible-light catalysis. Our findings could help to design new graphene derivative photocatalysts with high photocatalytic H_2 production performance and stability.

Acknowledgments

This work was supported by the National Major Basic Research Project of 2012CB934302, the National 863 Program2011AA050518, and the Natural Science Foundation of China (grant nos. 11174197 and 61234005).

References

[1] Fujishima A and Honda K 1972 Electrochemical photolysis of water at a semiconductor electrode *Nature* **238** 37–8
[2] Chen X B, Shen S H, Guo L J and Mao S S 2010 Semiconductor-based photocatalytic hydrogen generation *Chem. Rev.* **110** 6503–70
[3] Hong Y, Zhang J, Wang X, Wang Y, Lin Z, Yu J and Huang F 2012 Influence of lattice integrity and phase composition on the photocatalytic hydrogen production efficiency of ZnS nanomaterials *Nanoscale* **4** 2859–62
[4] Zhang J, Wang Y, Zhang J, Lin Z, Huang F and Yu J 2012 Enhanced photocatalytic hydrogen production activities of Au-loaded ZnS flowers *ACS Appl. Mater. Interfaces* **5** 1031–7
[5] Zhang J, Yu J G, Zhang Y M, Li Q and Gong J R 2011 Visible light photocatalytic H-2-production activity of CuS/ZnS porous nanosheets based on photoinduced interfacial charge transfer *Nano Lett.* **11** 4774–9
[6] Arai T, Senda S-I, Sato Y, Takahashi H, Shinoda K, Jeyadevan B and Tohji K 2008 Cu-doped ZnS hollow particle with high activity for hydrogen generation from alkaline sulfide solution under visible light *Chem. Mater.* **20** 1997–2000
[7] Kudo A and Sekizawa M 2000 Photocatalytic H_2 evolution under visible light irradiation on Ni-doped ZnS photocatalyst *Chem. Commun.* **15** 1371–2

[8] Tsuji I and Kudo A 2003 H_2 evolution from aqueous sulfite solutions under visible-light irradiation over Pb and halogen-codoped ZnS photocatalysts *J. Photo. Chem. Photobiol.* A **156** 249–52

[9] Zhang K, Jing D, Chen Q and Guo L 2010 Influence of Sr-doping on the photocatalytic activities of CdS–ZnS solid solution photocatalysts *Int. J. Hydrog. Energy* **35** 2048–57

[10] Wang D H, Wang L and Xu A W 2012 Room-temperature synthesis of $Zn_{0.80}Cd_{0.20}S$ solid solution with a high visible-light photocatalytic activity for hydrogen evolution *Nanoscale* **4** 2046–53

[11] Xu M, Zai J, Yuan Y and Qian X 2012 Band gap-tunable $(CuIn)_xZn_{2(1-x)}S_2$ solid solutions: preparation and efficient photocatalytic hydrogen production from water under visible light without noble metals *J. Mater. Chem.* **22** 23929–34

[12] Deshpande A, Shah P, Gholap R S and Gupta N M 2009 Interfacial and physico-chemical properties of polymer-supported CdS·ZnS nanocomposites and their role in the visible-light mediated photocatalytic splitting of water *J. Colloid Interface Sci.* **333** 263–8

[13] Zhang J, Yu J, Jaroniec M and Gong J R 2012 Noble metal-free reduced graphene oxide-$Zn_xCd_{1-x}S$ nanocomposite with enhanced solar photocatalytic H_2-production performance *Nano Lett.* **12** 4584–9

[14] Li Q, Meng H, Zhou P, Zheng Y, Wang J, Yu J and Gong J 2013 $Zn_{1-x}Cd_xS$ solid solutions with controlled bandgap and enhanced visible-light photocatalytic H_2-production activity *ACS Catal.* **3** 882–9

[15] Chen H M, Chen C K, Liu R-S, Wu C-C, Chang W-S, Chen K-H, Chan T-S, Lee J-F and Tsai D P 2011 A new approach to solar hydrogen production: a ZnO–ZnS solid solution nanowire array photoanode *Adv. Energy Mater.* **1** 742–7

[16] Huang L, Wang X, Yang J, Liu G, Han J and Li C 2013 Dual cocatalysts loaded type I CdS/ZnS core/shell nanocrystals as effective and stable photocatalysts for H_2 evolution *J. Phys. Chem.* C **117** 11584–91

[17] An X Q and Yu J C 2011 Graphene-based photocatalytic composites *RSC Adv.* **1** 1426–34

[18] Huang X, Qi X Y, Boey F and Zhang H 2012 Graphene-based composites *Chem. Soc. Rev.* **41** 666–86

[19] Zhang N, Zhang Y H and Xu Y J 2012 Recent progress on graphene-based photocatalysts: current status and future perspectives *Nanoscale* **4** 5792–813

[20] Xie G, Zhang K, Guo B, Liu Q, Fang L and Gong J R 2013 Graphene-based materials for hydrogen generation from light-driven water splitting *Adv. Mater.* **25** 3820–39

[21] Julkapli N M and Bagheri S 2015 Graphene supported heterogeneous catalysts: an overview *Int. J. Hydrogen Energy* **40** 948–79

[22] Weng B, Yang M-Q, Zhang N and Xu Y-J 2014 Toward the enhanced photoactivity and photostability of ZnO nanospheres via intimate surface coating with reduced graphene oxide *J. Mater. Chem.* A **2** 9380–9

[23] Li H and Cui X 2014 A hydrothermal route for constructing reduced graphene oxide/TiO_2 nanocomposites: enhanced photocatalytic activity for hydrogen evolution *Int. J. Hydrog. Energy* **39** 19877–86

[24] Li Q, Guo B, Yu J, Ran J, Zhang B, Yan H and Gong J R 2011 Highly efficient visible-light-driven photocatalytic hydrogen production of CdS-cluster-decorated graphene nanosheets *J. Am. Chem. Soc.* **133** 10878–84

[25] Yang M-Q and Xu Y-J 2013 Selective photoredox using graphene-based composite photocatalysts *Phys. Chem. Chem. Phys.* **15** 19102–18

[26] Yang J H, Wang D G, Han H X and Li C 2013 Roles of cocatalysts in photocatalysis and photoelectrocatalysis *Acc. Chem. Res.* **46** 1900–9

[27] Zhang Y H, Zhang N, Tang Z R and Xu Y J 2012 Graphene transforms wide band gap ZnS to a visible light photocatalyst. The new role of graphene as a macromolecular photosensitizer *ACS Nano* **6** 9777–89

[28] Hummers W S and Offeman R E 1958 Preparation of graphitic oxide *J. Am. Chem. Soc.* **80** 1339

[29] Zhang N, Yang M-Q, Tang Z-R and Xu Y-J 2013 Toward improving the graphene-semiconductor composite photoactivity via the addition of metal ions as generic interfacial mediator *ACS Nano* **8** 623–33

[30] Dahn J R, Sleigh A K, Shi H, Reimers J N, Zhong Q and Way B M 1993 Dependence of the electrochemical intercalation of lithium in carbons on the crystal structure of the carbon *Electrochim. Acta* **38** 1179–91

[31] Hu H T, Wang X B, Liu F M, Wang J C and Xu C H 2011 Rapid microwave-assisted synthesis of graphene nanosheets-zinc sulfide nanocomposites: optical and photocatalytic properties *Synth. Met.* **161** 404–10

[32] Ferrari A C 2007 Raman spectroscopy of graphene and graphite: disorder, electron-phonon coupling, doping and nonadiabatic effects *Solid State Commun.* **143** 47–57

[33] Graf D, Molitor F, Ensslin K, Stampfer C, Jungen A, Hierold C and Wirtz L 2007 Spatially resolved Raman spectroscopy of single- and few-layer graphene *Nano Lett.* **7** 238–42

[34] Casiraghi C, Hartschuh A, Qian H, Piscanec S, Georgi C, Fasoli A, Novoselov K S, Basko D M and Ferrari A C 2009 Raman spectroscopy of graphene edges *Nano Lett.* **9** 1433–41

[35] Kudin K N, Ozbas B, Schniepp H C, Prud'homme R K, Aksay I A and Car R 2008 Raman spectra of graphite oxide and functionalized graphene sheets *Nano Lett.* **8** 36–41

[36] Leary R and Westwood A 2011 Carbonaceous nanomaterials for the enhancement of TiO_2 photocatalysis *Carbon* **49** 741–72

[37] Park Y, Kim W, Park H, Tachikawa T, Majima T and Choi W 2009 Carbon-doped TiO_2 photocatalyst synthesized without using an external carbon precursor and the visible light activity *Appl. Catal.* B **91** 355–61

[38] Zeng P, Zhang Q, Peng T and Zhang X 2011 One-pot synthesis of reduced graphene oxide-cadmium sulfide nanocomposite and its photocatalytic hydrogen production *Phys. Chem. Chem. Phys.* **13** 21496–502

[39] Zhang H, Lv X, Li Y, Wang Y and Li J 2010 P25-graphene composite as a high performance photocatalyst *ACS Nano* **4** 380–6

[40] Woan K, Pyrgiotakis G and Sigmund W 2009 Photocatalytic carbon-nanotube- TiO_2 composites *Adv. Mater.* **21** 2233–9

[41] Kim C H, Kim B H and Yang K S 2012 TiO_2 nanoparticles loaded on graphene/carbon composite nanofibers by electrospinning for increased photocatalysis *Carbon* **50** 2472–81

[42] Bai X J, Wang L and Zhu Y F 2012 Visible photocatalytic activity enhancement of $ZnWO_4$ by graphene hybridization *ACS Catal.* **2** 2769–78

[43] Du A J, Ng Y H, Bell N J, Zhu Z H, Amal R and Smith S C 2011 Hybrid graphene/titania nanocomposites: interface charge transfer, hole doping, and sensitization for visible light response *J. Phys. Chem. Lett.* **2** 894–9

[44] Du A J *et al* 2012 Hybrid graphene and graphitic carbon nitride nanocomposites: gap electron–hole puddle, interfacial charge transfer, and enhanced visible light response *J. Am. Chem. Soc.* **134** 4393–7